Acta Geotechnica
https://doi.org/10.1007/s11440-020-01058-9

RESEARCH PAPER

Physical modeling of buried PVC pipes overlying localized ground subsidence

Yuri D. J. Costa[1] · Jorge G. Zornberg[2] · Carina M. L. Costa[1]

Received: 20 April 2020 / Accepted: 11 August 2020
© Springer-Verlag GmbH Germany, part of Springer Nature 2020

Abstract

The last half-century has witnessed a proliferation in the use of polyvinyl chloride (PVC) pipes in civil engineering applications. However, little physical data are available to date to assess conformance with performance limits of these pipes subjected to events involving localized ground subsidence. In this study, experimental results are generated and evaluated from a series of physical models involving a buried PVC pipe overlying a localized subsiding bedding zone. Ground subsidence was simulated using a precisely controlled trapdoor system positioned at mid-length of the pipe. A technique including the use of a custom-made displacement transducer was developed as part of this study to facilitate collection of continuous deflection profiles along the axis of the pipes. The progressive development of soil arching was also monitored using earth pressure sensors placed on the top, sides, and at several locations beneath the pipe, both within and beyond the zone of ground subsidence. Strains in the external wall of the pipe were also monitored. The results indicate that significant bending developed in the portion of the pipe traversing the subsidence zone, especially at the pipe crown. Beyond this point, radial deflections of the pipe cross section continued to be detected along the pipe length to distances of approximately four pipe diameters. Ground subsidence induced a severe redistribution of the earth pressures measured in the soil mass surrounding the pipe. A significant increase in vertical soil pressures beneath the pipe was captured within a distance of about one pipe diameter outside the subsidence zone. The overall response of the PVC pipe to localized ground subsidence was found to improve with increasing backfill density and decreasing soil confinement.

Keywords Ground subsidence · Physical modeling · PVC pipe · Soil arching · Trapdoor

List of symbols

A	Area of pipe wall per unit length of pipe (m^2/m)
B	Width of the trapdoor (m)
C_n	Calibration factor
D	External diameter of the pipe (m)
D_r	Soil relative density (%)
E_p	Elastic modulus of pipe material (GPa)
H	Soil cover thickness above pipe crown (m)
I_p	Moment of inertia of the pipe wall per unit length (m^4/m)
K	Lateral earth pressure coefficient
K_a	Rankine's active earth pressure coefficient
K_{kr}	Krynine's earth pressure coefficient
L	Length of the trapdoor (m)
M_s	Secant constrained soil modulus (MPa)
PS	Pipe stiffness (kN/m/m)
R	Radius from the center of the pipe to the centroid of the pipe profile (m)
R_H	Correction factor for backfill soil geometry
S_H	Hoop stiffness factor
q	External surcharge pressure (kPa)
t	Pipe wall thickness (mm)
w	Geometry coefficient (m^{-1})
Δ	Pipe radial deflection (%)
Δ_T	Pipe total deflection (%)
γ	Soil unit weight (kN/m^3)
δ	Trapdoor vertical displacement (m)

✉ Yuri D. J. Costa
ydjcosta@ct.ufrn.br

Jorge G. Zornberg
zornberg@mail.utexas.edu

Carina M. L. Costa
carina@ct.ufrn.br

[1] Department Civil Engineering, Federal University of Rio Grande do Norte, Av. Sen. Salgado Filho, 3000, Natal, RN 59072-970, Brazil

[2] Department of Civil, Architectural and Environmental Engineering, The University of Texas at Austin, 301 E. Dean Keeton St., Stop C1792, Austin, TX 78712-1174, USA

Published online: 05 September 2020

ε	Pipe wall strain
ε_{bck}	Limit strain for buckling
ε_{yc}	Maximum compressive strain
ε_{yt}	Maximum service long-term tension strain
ν_s	Poisson ratio of the soil
σ_h	Horizontal pressure in the soil (kPa)
σ_{ho}	Horizontal pressure prior to yielding of the buried structure (kPa)
σ_v	Vertical pressure in the soil (kPa)
σ_{vo}	Vertical pressure prior to yielding of the buried structure (kPa)
ϕ	Internal friction angle of the soil (°)
ϕ_{bck}	Resistance factor for global buckling

1 Introduction

Many of the pipeline failures identified in the recent literature point to problems related to interactions along the longitudinal direction of pipes. Excessive pipeline strains as well as failure in the form of cracking or buckling may be consequences of longitudinal interactions. A circumferential failure in a pipe is usually a result of an extreme longitudinal tensile stress condition. Benmansour et al. [4] evaluated data from sewer lines in Nice, France, which total 850 km in length and involve primarily reinforced concrete pipes. Circumferential cracks and fissures, resulting from longitudinal bending of the pipeline, were found to be the most common type of structural defects (15.7% of the total pipeline system). Based on data from several US and Canadian cities, Rajani et al. [27] found that an average of 70% of water main failures are circumferential. More recently, a comprehensive water main failure rate study, including data covering 274,504 km of pipes in the USA and Canada, was provided by [11]. The study identified that circumferential cracks are responsible for 37% of catalogued failure modes, followed by corrosion-related problems at 27%. Longitudinal cracks and other occurrences respond for the remaining causes of failure.

Some factors that trigger pipe longitudinal interactions are related to the localized subsidence of the supporting ground, which may cause the pipe to settle. Particularly, a localized ground subsidence in a pipe can be triggered by various factors, such as mine subsidence [25, 40], presence of faults in the pipe alignment [6, 24, 28, 39], faulty workmanship [3], internal erosion [12, 18, 26], lowering of the groundwater table [32] and tunneling operations [37, 38, 43].

A number of laboratory models have been developed to understand the behavior of pipes undergoing subsidence. Model pipes of different stiffness values, representing the broad spectrum of rigid and flexible systems fabricated with different materials, have been evaluated experimentally. Studies involving hollow and solid cross-section model pipes made of polytetrafluoroethylene (PTFE), polycarbonate, high-density corrugated polyethylene, Nylon, Perspex, acrylic, aluminum and steel have been identified in the technical literature [6, 21, 24, 28, 29, 37, 44]. Although the last half-century has witnessed the proliferation of polyvinyl chloride (PVC) pipes, similar experimental investigations involving PVC model pipes remain scarce. The increasing usage of PVC pipes in engineering practice, as described by Cohen [7] and Folkman [11], underscores the importance of understanding the deformation limits that these pipes could bear as a consequence of localized subsidence.

To simulate ground subsidence, models have typically employed a trapdoor system beneath the pipe, composed of either a single [13, 24, 28, 36] or a series of movable contiguous plates that were lowered to different levels [38, 44]. Some models have involved an inclined trapdoor mounted to simulate reverse faults [6]. In all these models, the trapdoor was used to represent an unstable zone covering a comparatively large area below the pipe. That was because most investigations focused on ground deformations caused by earthquake faults or tunneling, which involve widespread subsiding zones in the ground. However, problems involving the subsidence of comparatively small areas below the pipe (e.g., induced by sinkholes or internal erosion) may also be particularly relevant and lead to different displacement and failure patterns.

The descent of the trapdoor during testing has generally been achieved by regulating the discharge of oil from a hydraulic cylinder. However, precise control of the trapdoor displacements was often compromised with this approach, even if the displacements were applied in stages. Alternatively, some pipeline models simulating their crossing of tunnels induced pipe settlements by removing water from a latex membrane lining a rigid mandrel used to represent a tunnel [21, 37]. This method may similarly lead to imprecise control of the pipe subsidence.

Since a flexible pipe derives the soil carrying capacity from its flexibility [15], deflection is the most important variable in the design of flexible pipes, such as the class of PVC pipes. Accurate pipe deflection measurements in physical models are therefore crucial to adequately understand the actual behavior of flexible pipes. Zhou et al. [44] used settlement plates to monitor the vertical displacements at the crown of model pipes. Although effective, a disadvantage of this approach is that measurements are limited to a few specific positions at the crown of the

pipe. Another method to measure pipe deflections has been the use of techniques involving image collection and analysis or the measurements of strains on the pipe walls. The image processing technique referred to as digital image correlation (DIC) has achieved widespread acceptance [42]. Particle image velocimetry (PIV) analysis has been used to track the deflected shape of halved pipeline models placed against transparent test container walls [6, 21, 28, 29]. However, sidewall friction is known to restrict the displacement of sand particles in contact with the transparent wall of soil models [5, 30]. In buried pipe models, sidewall friction may directly interfere with the development of movements in the halved pipe model placed against the transparent wall and potentially induce significant errors in image analysis techniques, such as PIV. Alternatively, some experimental investigations have obtained model pipe deflections by recording the strain distribution along the pipe via strain gages attached to the pipe's external surface [24, 29, 36, 37]. Curve fitting of the strain readings and subsequent integration along the pipe axis has been used to obtain pipe deflections. Since strain gages give point measurements of strains, many gages are necessary to produce deflection profiles without significant distortions. However, the number of strain gages used in the model pipe may be limited for various reasons, such as space availability in the model pipe, number of channels for the data acquisition system and cost. Furthermore, attaching too many strain gages may interfere with the actual behavior of a flexible model pipe due to local stiffening of the pipe surface caused by the bonding resin. Consequently, an opportunity exists to employ a technique that produces continuous deflection profiles of model pipes subjected to ground subsidence.

Considering the assessment of the previous investigations conducted on the topic, the aim of the research reported in this paper is to analyze data from physical models involving a PVC pipe embedded in a granular soil and subjected to localized subsidence in the underlying soil. Pipe and soil displacements were induced in the models by a precisely controlled trapdoor system. A custom-made transducer was developed to obtain deflection profiles along the length of the model pipe. The deflection profiles from eight different positions in the pipe cross section were recorded throughout the subsiding process. Of particular relevance is that soil stresses were measured at the crown and springlines of the pipe, as well as at several locations beneath the pipe. Finally, changes in longitudinal and circumferential strains in the external wall of the model pipes were monitored using strain gages.

The paper initially describes the testing apparatus and procedures adopted for model preparation. Details about the transducer device developed as part of this study to accurately measure pipe deflections is then explained. An assessment of the deflections measured along the pipe axis and of the strains in the external pipe walls is subsequently presented. An analysis is made on soil stresses in the vicinity of the pipe, which includes comparisons to those predicted using analytical solutions. The paper concludes with a discussion of the results and overall findings.

2 Physical models of buried PVC pipes

2.1 Materials

The soil used in this study was a poorly graded sand (SP) with spherical particles ranging in size from 0.07 to 2 mm (medium to fine sand). The sand has a specific gravity of 2.65, a coefficient of uniformity of 2.7 and an average diameter of the grains (D_{50}) of 0.23 mm. The sand was characterized by minimum and maximum dry unit weights of 14.2 kN/m^3 and 17.7 kN/m^3, respectively. Additional information about the used sand can be found in [9].

Commercially available solid-wall PVC pipes with an external diameter (D) of 75 mm, wall thickness (t) of 2 mm and length of 1395 mm were used in the reduced-scale model tests. A new specimen was used for each test. The mechanical properties of the model pipes were obtained from compression parallel-plate tests performed according to ASTM D 2412-11 [2]. Pipe specimens measuring 150 mm in length were tested in a universal testing machine with a maximum load capacity of 30 kN, operating at a displacement rate of 12.5 mm/min. The pipe stiffness (PS), calculated from the parallel plate test results for a deflection of 5% [41], equals 192 kN/m/m. A Young's modulus of elasticity of 2.09 GPa was obtained for the pipe material (E_p), after back-analysis of the following equation [41]:

$$\mathrm{PS} = 53.6\frac{E_p I_p}{D^3} \tag{1}$$

where E_p is the modulus of elasticity of the pipe material; I_p is the moment of inertia of the pipe wall per unit length $\left(I_p = t^3/12\right)$; and D is the pipe diameter.

Foil strain gages were used to monitor the development of strains in the external wall of two model pipes. The strain gages were attached to the crown, invert and one of the springlines of the mid-length section of the pipe. The strain gages had a resistance of 350 Ω and grid dimensions measuring 9.53 mm in length and 3.18 mm in width. Each instrumented point on the model pipe had two strain gages individually connected to form a quarter Wheatstone bridge circuit. The gage units were bonded to the surface of the pipe, with the grid length aligned either parallel or perpendicular to the pipe axis to measure axial or circumferential strains in the pipe wall, respectively. A layer

of silicone rubber and insulation tape was used to provide the strain gages with mechanical protection during testing. Pipe deflections and soil stresses were not measured in the models constructed using a strain-gage instrumented pipe.

2.2 Model container and trapdoor system

The tests were conducted in a rigid metal container with interior dimensions of 1400 mm length, 560 mm height and 560 mm width. Longitudinal and transverse cross-section views of the model container are shown in Fig. 1a, b, respectively.

Pipe settlements were triggered by a trapdoor system, which measured 100 mm in width and 300 mm in length, situated at the center of the model. The system consisted of three stainless steel prisms, 120 mm in height, which ascended or descended simultaneously via a precisely controlled threaded axis driven by gears and connected to a hand crank. Two linear variable displacement transformers (LVDT), mounted below the test container, were used to monitor the vertical displacements of the trapdoor. The displacement transformers had a maximum stroke of 50 mm and a resolution of 0.01 mm.

Total pressures were measured in the models using miniature earth pressure sensors with a 23-mm-diameter sensing surface, 5.7 mm in thickness. Earth pressures were measured from 0 to 200 kPa with a resolution of 1% at 200 kPa.

The sensors labeled as units M1 to M6 were placed at the crown and springlines of the pipe, at two distinct sections of the model. As shown in the schematic presented in Fig. 1a, Section S1 is at the center of the model and Section S2 intersects one edge of the trapdoor. Additionally, four interface pressure sensors with the same characteristics of those displaced in the soil mass were installed below the pipe (units I1 to I4), in slots flush with the floor of the container: unit I1 was located within the trapdoor, at its center, while units I2, I3 and I4 were located outside the limits of the trapdoor (Fig. 1a). The distances of sensors I2, I3 and I4 from the central sensor are, respectively, 170 mm, 223 mm and 421 mm.

2.3 Displacement transducer

Deflections of the model pipe were recorded by a strain gage-based transducer device built specifically for this investigation. The device consisted of eight spring steel arms, with cross sections 6 mm wide and 0.2 mm thick, mounted in a cylindrical aluminum base with 35 mm in diameter and 40 mm in length, as shown in Fig. 2a. The transducer was able to simultaneously record displacements at eight distinct positions, 45° apart, along the pipe cross-sectional circumference. Each arm was equipped with two 120-Ω strain gages bound to the back and front of the arm and connected in a half bridge circuit. Bending of the arm generates tension on the upper strain gage and compression on the lower strain gage, so that the strains recorded by both sensors were of equal magnitude and opposite sign. Because the arms were manufactured of a homogeneous and isotropic material, the resulting output signal was doubled and any effect of temperature on the strain output was canceled out. A photograph of the custom-made transducer is shown in Fig. 2b.

The transducer moved along the longitudinal axis of the pipe by sliding through an aluminum guide rod with a square cross section, as shown in Fig. 1a. A detail of the displacement transducer moving system built for the experiments is presented in Fig. 1c. The error of the displacement measurements was $\pm$ 0.02 mm. The guide rod was secured outside the box by two supports equipped with threaded spindles to facilitate alignment with the pipe's longitudinal axis. A stepper motor, installed on one of the supports, pulled the transducer inside the pipe at a constant speed. When the base of the transducer made contact with a stopper located at the inbound edge of the guide rod, power to the motor was cut off. Friction during movement was minimized by a steel ball bearing bonded to each arm of the transducer at the point of contact with the pipe wall. In addition, graphite powder was used to lubricate the contact between the aluminum guide and transducer base.

2.4 Model preparation and scope of the testing program

Carefully controlled construction procedures were followed during model preparation. The models were prepared at target soil densities by pluviating air-dried sand (moisture content below 1%) into the test box under controlled discharge heights and rates. Model construction began with placement of a 30-mm-thick bedding layer to support the model pipe. A vacuum system was used to achieve the target layer elevation, which consisted of a calibrated metallic tube into which vacuum was applied to remove any excess pluviated sand. The model pipe was placed over the bedding layer, and following assembly of the deflection measurement system inside the pipe and attachment of the earth pressure sensors to its external wall, sand pluviation was resumed in the container. During model preparation, visual inspections were proceeded to ensure a complete filling around the pressure sensors. After the box was completely filled, the final surface of the model was carefully leveled using the vacuum system. The internal walls of the container were coated with two layers of 0.075-mm-thick polyester film to minimize the effects of side friction. A PVC bladder was placed on top of the model in order to apply a constant distributed external

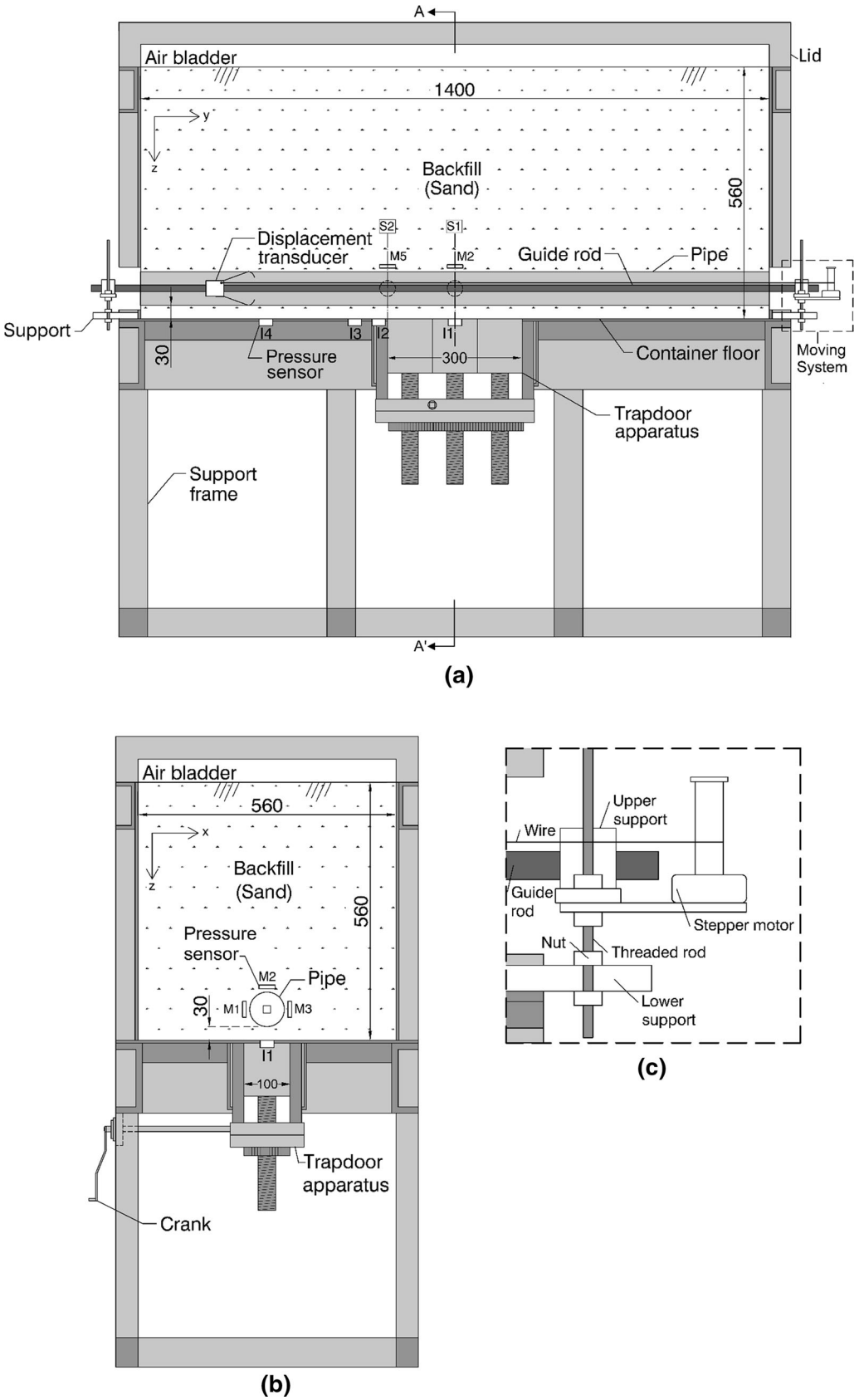

◀**Fig. 1** Schematic diagram of a model pipe: **a** longitudinal cross-section view; **b** transverse cross-section view; and **c** detail of transducer moving system (units: mm)

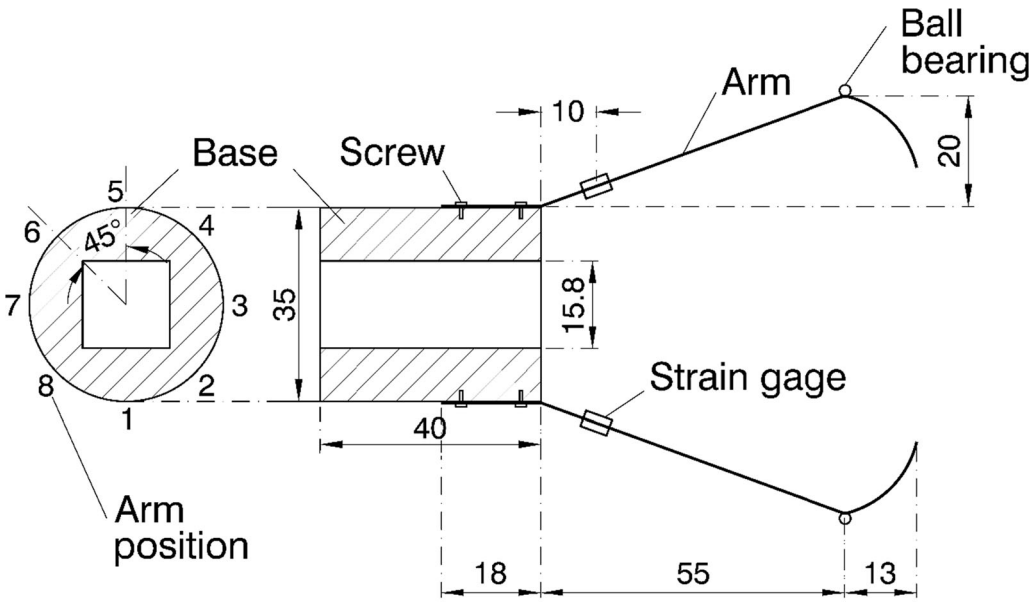

(a)

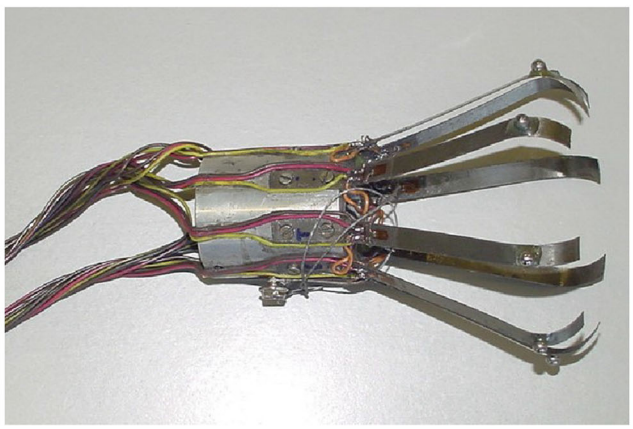

(b)

Fig. 2 Displacement transducer: **a** schematic view (units: mm) and **b** photograph of the transducer

surcharge to the backfill during testing. The high flexibility of the pressure bladder's manufacturing material contributed to minimizing stress concentrations at the center of the model. The bladder reacted against a metal lid that was securely fastened to the testing box with bolts (see Fig. 1a, b).

The deflection profiles and total stresses within the soil mass were measured at specific displacements of the underlying trapdoor while applying the target surcharge. Each deflection profile presented herein corresponds to the mean of four identical repeat runs of the displacement transducer. The transducer output signals were collected by a data acquisition system and recorded on a microcomputer for subsequent processing.

The scope of the testing program is summarized in Table 1. The models were built to sand relative densities (D_r) of 50, 75 and 100%, representing loose, intermediate and compact backfills, respectively. The tests were conducted under external surcharge values (q) ranging from 0 to 150 kPa. Tests 8 and 9 were carried out using the pipes instrumented with strain gages to measure strains in the pipe wall. Tests 10 and 11 were conducted without a pipe, for the purpose of comparing the development of earth pressures against those in models constructed with pipes.

Table 1 Summary of model tests

	Model test										
	1	2	3	4	5	6	7	8[a]	9[a]	10[b]	11[b]
Relative density, D_r (%)	100	100	100	75	50	50	50	50	100	50	100
External surcharge, q (kPa)	50	100	150	100	50	100	150	100	100	100	100

[a]Test with pipe instrumented with strain gages

[b]Test without pipe

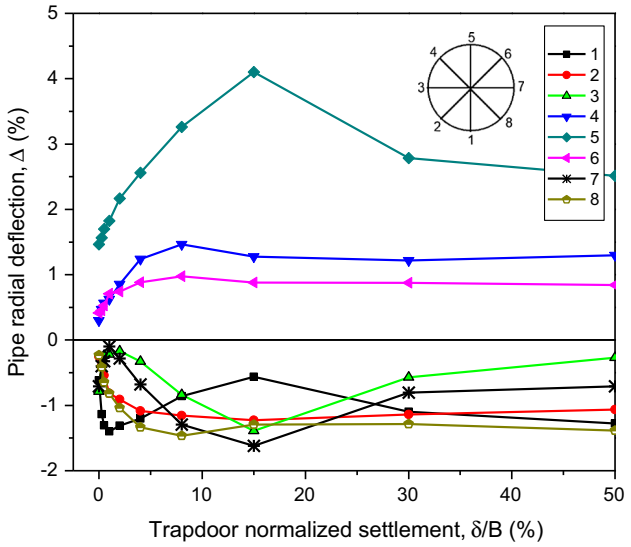

Fig. 3 Radial deflections in Model 6 (Section S1) obtained with increasing normalized trapdoor settlements

3 Evaluation of pipe deflections

Typical results obtained following testing of Model 6 are initially presented to illustrate the type of information gathered throughout the study for each model pipe undergoing localized subsidence. Figure 3 shows the variation in deflection (Δ) in the pipe's central cross section S1 obtained for increasing trapdoor settlements (δ). The pipe deflection is defined as the radial displacement measured at each one of the eight circumferential positions (CP) along the cross section, normalized by the pipe diameter. Negative values of Δ correspond to outward displacements (i.e., away from the pipe center). This way of reporting deflections differs from the use of total deflections (Δ_T), which is the sum of the deflections from two diametrically opposed positions in the pipe diameter [15]. In this study, the settlement of the trapdoor (δ) is reported as a percentage of the trapdoor width (B).

The trapdoor settlements induced large deflections on the pipe central cross section (S1), which included sagging of the crown, upheaval of the invert and extension of the horizontal diameter. The most critical condition for the pipe was achieved at δ/B = 15%, while stable, residual conditions were achieved beyond δ/B = 30%. Deflections were significantly larger at the crown of the pipe (CP5) as compared to the other circumferential positions in cross section S1. The settlement of the trapdoor caused a significant, progressively inward deflection of the crown, which reached its peak at δ/B = 15%. While smaller than that at the crown of the pipe, the shoulders of the pipe (CP4 and CP6) also experienced inward deflections.

The trapdoor increasing settlement values produced a sequence of alternate inward and outward deflections of the invert and springlines of the pipe. Deflections of the invert (CP1) followed an outward–inward–outward path. Initially, the trapdoor translation caused the pipe invert to settle sharply, but between the normalized displacements of 1% and 15%, the invert experienced heave and then continued to show settlements. In contrast, deflections of the springlines (CP3 and CP7) followed an inward–outward–inward path. The initial settlement of the trapdoor produced a prominent shortening along the pipe's horizontal diameter. However, for normalized trapdoor settlements ranging between δ/B = 1% and 15%, deflections reversed and the pipe experienced an increase along the pipe's horizontal diameter. An additional reduction in the pipe diameter at the springlines occurred beyond δ/B = 15%.

Profiles of radial deflections along the pipe axis for the different circumferential points (CP1 to CP8) at normalized trapdoor settlements of 15% and 50% are shown in Fig. 4a, b, respectively. The results indicate that once the trapdoor reached a relative settlement δ/B = 15%, the influence of the subsidence zone on pipe deflections extends to approximately four pipe diameters beyond the trapdoor limits (Fig. 4a). Sagging of the crown (CP5) and shoulders (CP4 and CP6) occurred in the region where the pipe crossed the trapdoor. Sagging reached its maximum magnitude at the central cross section S1 and gradually attenuated beyond the trapdoor zone. The outward deflections of the springlines (CP3 and CP7) and haunches (CP2 and CP8) also reached their maximum at the central cross section S1. The profile of the pipe invert (CP1) developed a peculiar "W" shape: a downward concavity above the

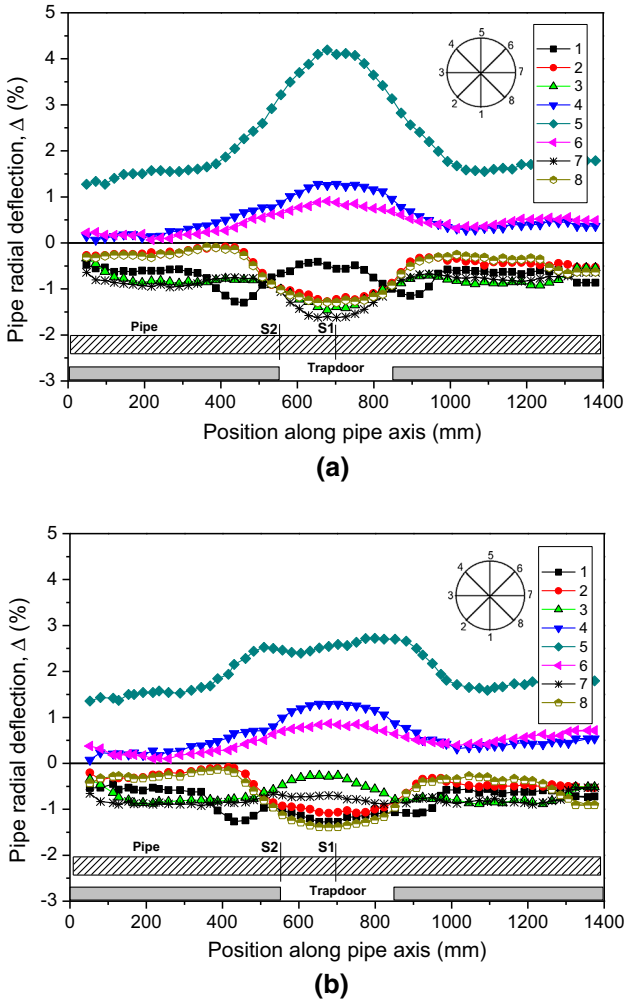

Fig. 4 Profiles of radial deflections in Model 6 along pipe axis: **a** at a normalized trapdoor settlement δ/B = 15% and **b** at a normalized trapdoor settlement δ/B = 50%

trapdoor and upward concavities beyond the trapdoor limits.

Profiles at a trapdoor relative settlement δ/B = 50% showed comparatively smaller deflections in the region above the trapdoor (Fig. 4b). Specifically, deflections of the pipe crown were significantly smaller and deflections of the springlines reverted in relation to those observed at a trapdoor relative settlement δ/B = 15%. Furthermore, the downward concavity of the invert above the trapdoor vanished, but the upward concavity beyond the trapdoor limits remained.

Figure 5 compares the profiles of deflection reached using a backfill with a relative density (D_r) of 50% with those obtained at using a backfill with a relative density of 100%, which represent loose and dense compaction conditions, respectively. Both sets of profiles correspond to a trapdoor relative settlement δ/B = 15% and an applied external surcharge of 100 kPa. For clarity, only deflections

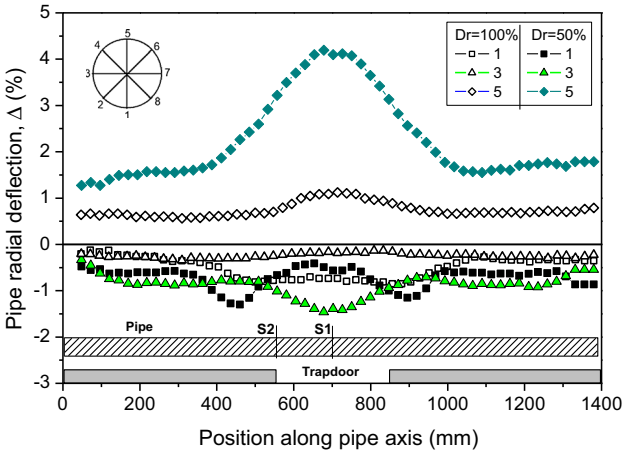

Fig. 5 Comparison of radial deflection profiles of pipes embedded in backfills with relative densities of 50% and 100%, at a normalized trapdoor displacement δ/B = 15%

of the crown, invert and one of the two springlines are displayed. As shown in the figure, radial deflections were significantly larger at the crown and slightly larger at the springlines of the pipe embedded in the loose backfill. The peculiar "W" shape at the invert of the pipe embedded in the loose backfill did not recur in the dense backfill. Instead, a slight, nearly flat sagging was observed along the pipe segment traversing the trapdoor, which extended to a horizontal distance of about 4 D beyond the trapdoor limits. The profiles presented in Fig. 5 agree with the patterns identified by Costa et al. [8] from image analysis of centrifuge models of half-sectioned buried pipes embedded in both loose and dense backfills.

Figure 6 compares the radial deflections obtained at Section S1 for the cases of pipes embedded in loose (D_r = 50%), intermediate (D_r = 75%) and dense (D_r = 100%) backfill soils, at selected trapdoor relative displacements. The radial deflections are shown for the various circumferential positions in the pipe cross section. The results in the figure indicate that the deflections obtained in pipes embedded in the dense and intermediate backfills were very similar and significantly smaller than those in the pipe embedded in the loose backfill. The influence of soil density was comparatively small for small trapdoor relative displacements (δ/B = 1% in Fig. 6a) and after reaching a residual condition (δ/B = 30% in Fig. 6c). However, soil density played a marked role on the pipe radial deflections at a trapdoor relative displacement δ/B = 15% (Fig. 6b).

The deformed shapes of pipe sections S1 and S2 embedded in loose, intermediate and dense backfills, at a trapdoor normalized displacement δ/B of 15%, are shown in Fig. 7. The magnitude of the radial deflection is indicated for each circumferential position. The displacements in the deformed pipe are magnified by a factor of 5 in the figure. Figure 7a, b, c presents the deformed shapes of

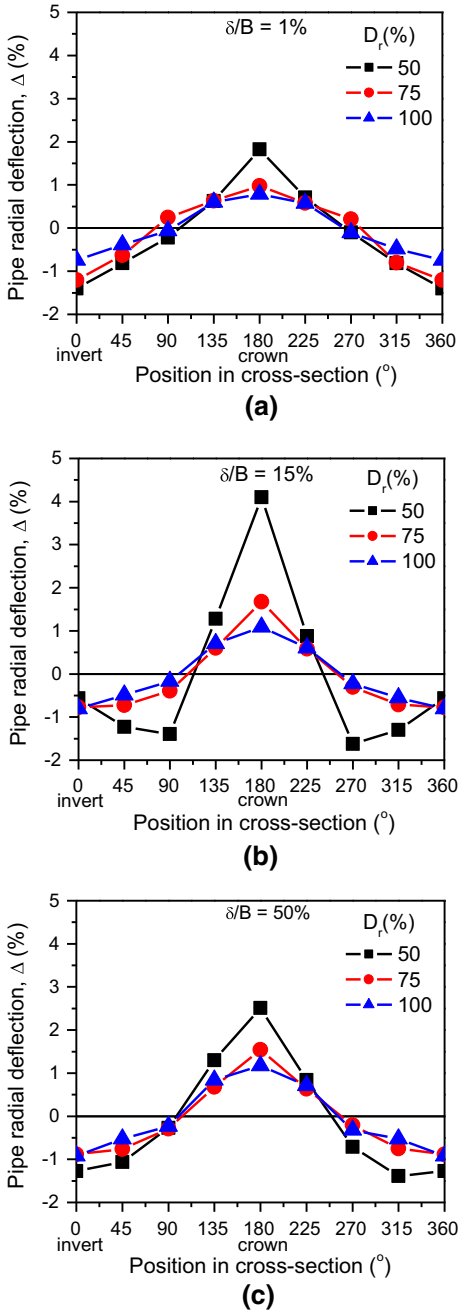

Fig. 6 Radial deflections at Section S1 of pipes embedded in backfills with different relative densities for different trapdoor normalized displacements: **a** δ/B = 1%; **b** δ/B = 15%; and **c** δ/B = 50%

central cross section S1 of the model pipes. The pipe embedded in the loose backfill soil was observed to develop a heart-like shape, characterized by a reversal of curvature at the crown and by flattening of the invert and haunches (Fig. 7a). The pipe diameter in the horizontal direction increased by 3%, while the diameter in the vertical direction decreased by 3.5%. Unlike the results obtained for the case of pipes embedded in loose backfill, the roundness of the pipes embedded in intermediate and dense backfills (Fig. 7b, c, respectively) was better preserved. The pipe in the intermediate backfill experienced some flattening at the top, but the radial deflection of the crown was comparatively smaller and did not show the reversal of curvature observed for the case of loose backfill. The deformed shapes of Section S2 of the model pipes, shown in Fig. 7c, d, e, were similar to those of Section S1. The observed deformed shapes agree with trends previously reported by Costa et al. [8] based on the results from centrifuge tests involving reduced-scale model pipes, and with the observations of Moser and Folkman [23] on plastic pipes.

Figure 8 presents the total vertical and horizontal deflections (Δ_T) of the pipe at Section S1, after ground subsidence, as a function of the external surcharge (q) for pipes embedded in backfills with different relative densities (D_r). Data are presented in terms of total deflection in this case to allow comparisons with deflection limits recommended in the literature. The data correspond to a trapdoor relative settlement δ/B of 15%, and best fit linear regressions are also shown in the figure. A decrease in the pipe diameter in the vertical direction is represented by positive values, while the increase in the pipe diameter in the horizontal direction is represented by negative values. As shown in the figure, the horizontal and vertical deflections induced by the imposed ground subsidence remained below the allowable total deflection limit usually adopted for thermoplastic pipes, which is 5% according to AASHTO [1]. The decrease in the diameter in the vertical direction slightly exceeded the increase in the diameter in the horizontal direction.

As expected, comparatively larger deflections were obtained in pipes embedded in backfills with lower relative densities and subjected to higher soil confinement levels. However, the impact of the surcharge level on Δ_T was found to be more significant for pipes embedded in loose backfill, as compared to those embedded in intermediate and dense backfills.

4 Evaluation of strains in the pipe wall

Development of strains (ε) in the pipe wall induced by ground subsidence is evaluated in this section. Figure 9 shows the variations in axial and circumferential strains on the pipe's outside wall collected via the strain gages attached to pipes at Section S1 in the crown (Fig. 9a), invert (Fig. 9b) and springlines (Fig. 9c). Both axial and circumferential strains measured in the tests include hoop and bending strains. Data were obtained from Models 8 and 9, built using loose (D_r = 50%) and dense (D_r = 100%) backfill soils, respectively, and subjected to the same applied surcharge of 100 kPa. Consistent with the sign

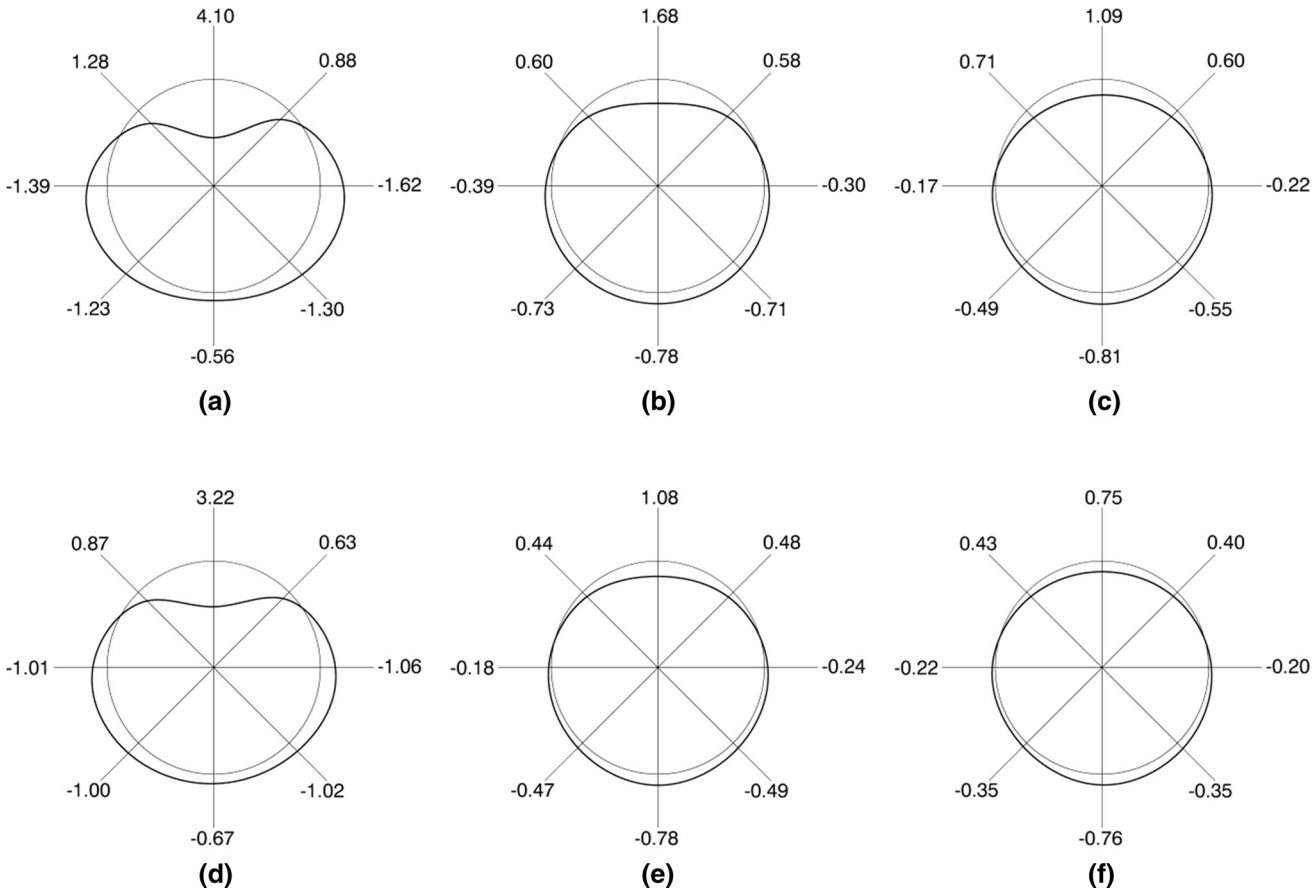

Fig. 7 Comparison of deformed shapes obtained from pipe sections: **a** Section S1, pipe embedded in a loose backfill (D_r = 50%); **b** Section S1, pipe embedded in an intermediate backfill (D_r = 75%); **c** Section S1, pipe embedded in a dense backfill (D_r = 100%); **d** Section S2, pipe embedded in a loose backfill (D_r = 50%); **e** Section S2, pipe embedded in an intermediate backfill (D_r = 75%); and **f** Section S2, pipe embedded in a dense backfill (D_r = 100%). (*Note*: percent radial deflection is indicated for each circumferential position)

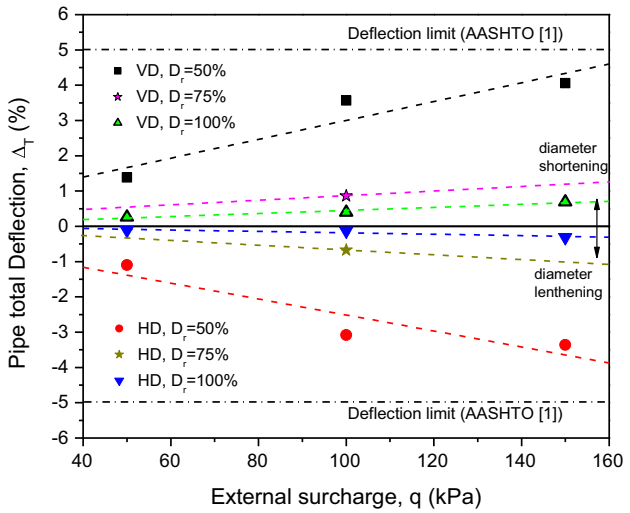

Fig. 8 Total pipe horizontal deflections (HD) and vertical deflections (VD) at Section S1 as a function of the external applied surcharge (q) for pipes embedded in backfills with different relative densities (D_r= 50%, 75% and 100%). *Note*: Pipe deflections correspond to those obtained at a trapdoor normalized displacement δ/B of 15%

convention adopted herein, compressive strains are represented as negative.

Most strain variations took place prior to trapdoor normalized settlements δ/B of 15%, which corresponds to the range of the largest changes in radial deflections. The pipe embedded in a dense backfill experienced comparatively lower circumferential and axial strains than that embedded in a loose backfill. In general, circumferential strains were larger than axial strains, particularly at the invert and springlines of the pipe.

Changes in radial deflections with increasing trapdoor displacements and along the pipe axis shown in Figs. 3, 4, 5, 6 and 7 are consistent with the interpretation of the trends presented in Fig. 9 for central cross section S1. For example, the compressive circumferential and axial strains at the pipe crown in Fig. 9a reflect the depression formed at this position upon subsidence. The circumferential strains at the pipe crown initially increased, then decreased and increased once more. The initial strain increase took place due to the elliptical shape assumed by Section S1 at small trapdoor settlements (i.e., shortening of the vertical

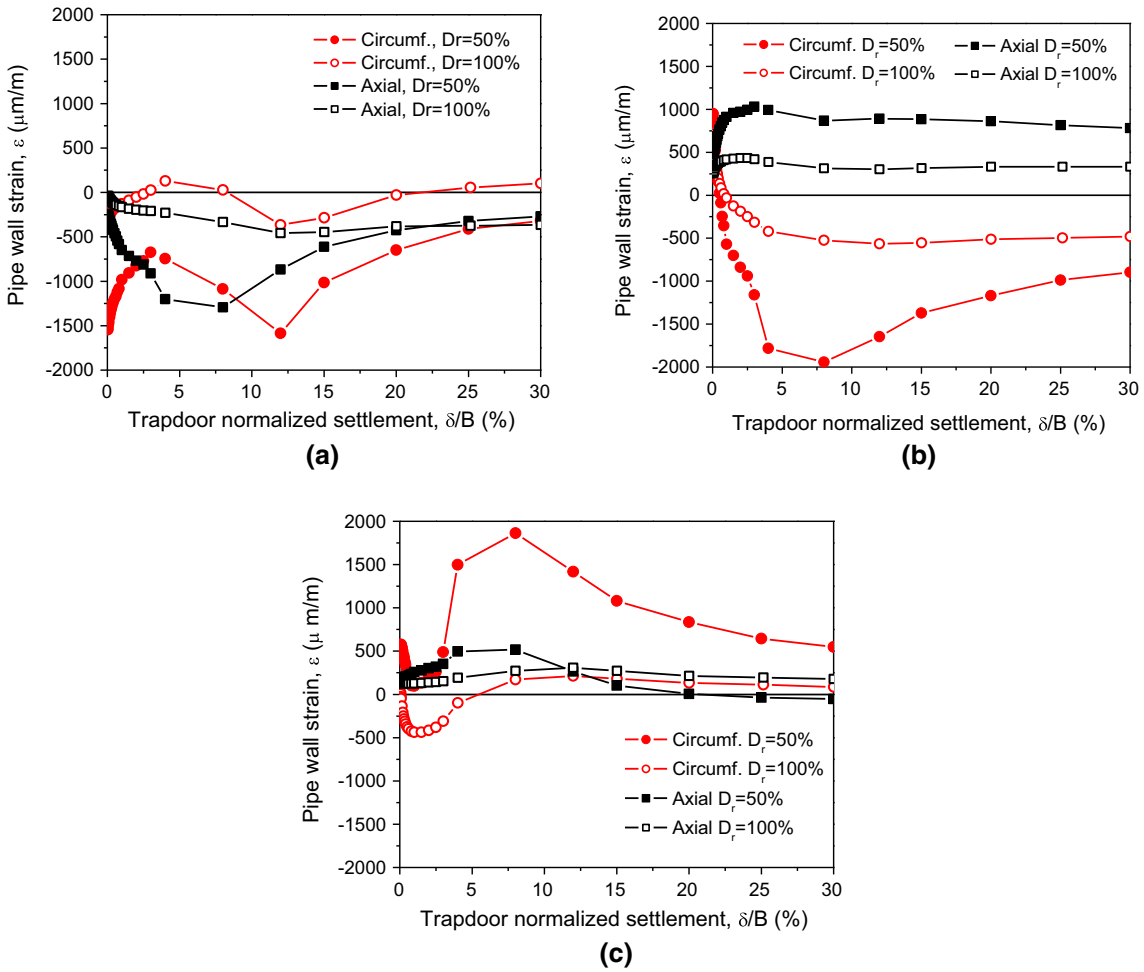

Fig. 9 Variations in circumferential and axial strains at Section S1 in the pipe wall induced by ground subsidence: **a** at the pipe crown; **b** at the pipe invert; and **c** at the pipe springline

diameter and lengthening of the horizontal diameter). With progression of trapdoor settlements, the pipe wall curvature at the crown reverted, as can be noted in Fig. 7, which led to a reduction in the measured circumferential strains. Finally, the direction of the deflections at the crown shifted at larger settlements (Fig. 3), which resulted in a new increase in circumferential strains. The increase in axial strains after an initial decrease resulted from the reduction in the longitudinal depression at the top of the pipe at larger trapdoor settlements, which followed an initial increase, as can be checked in the deflection profiles presented in Fig. 4a, b.

Pipeline design requires that strains in its walls remain below a certain limit value. For solid wall PVC pipes, AASHTO [1] specifies a maximum compressive strain of 2.6% (ε_{yc}) and a maximum service long-term tension strain of 5% (ε_{yt}). As confirmed by the results presented in Fig. 9, both peak compressive and tensile strains in the pipe models subjected to ground subsidence were below the limits given by [1]. Strains due to buckling should also be checked. According to AASHTO [1], compressive strains should not exceed the nominal strain capacity for general buckling, ε_{bck}, reduced by a resistance factor for global buckling, ϕ_{bck}, equal to 0.7. The buckling strain can then be calculated as follows [1]:

$$\varepsilon_{bck} = \frac{1.2C_n\left(E_pI_p\right)^{1/3}}{AE_p}\left[\frac{\phi_s M_s(1-2\nu_s)}{(1-\nu_s)^2}\right]^{2/3}\cdot R_H \qquad (2)$$

where C_n is a calibration factor to account for nonlinear effects, assumed as equal to 0.55 [1]; ϕ_s is the resistance factor for soil stiffness; M_s is the secant constrained soil modulus; ν_s is the Poisson ratio of the soil; E_p is the Young's modulus of pipe material; I_p is the moment of inertia of the pipe wall per unit length; A is the gross area of pipe wall per unit length of pipe; and R_H is a correction factor for backfill soil geometry, given in Eq. (3), with D and H in meters:

$$R_H = \frac{11.4}{11+\frac{D}{H}} \qquad (3)$$

Following AASHTO's [1] recommendations, the quantities C_n and ϕ_s in Eq. (2) were set to 0.55 and 0.9, respectively. Values for the constrained soil modulus (M_s) were selected from the range of values recommended by AASHTO's method for compacted sands, taking into consideration the external surcharge level and soil relative density used in the experiments. Specifically, the values of M_s were obtained for a surcharge level of 100 kPa and soil compaction degrees as a percentage of dry unit weight equal to 90% and 100%, which correspond to relative densities of 50% and 100%, respectively. Since the exact surcharge level of 100 kPa was not available in the method's database, corresponding values of M_s for q = 100 kPa were obtained by interpolation. The chosen values were M_s = 11.8 MPa for Model 8 (D_r = 50%) and M_s = 33.5 MPa for Model 9 (D_r = 100%) (see Table 3). The soil Poisson ratio was taken as 0.35 for both models.

According to Eq. (2), $0.7\varepsilon_{bck}$ equals 0.49% for a backfill relative density of 50% and 0.97% for a backfill relative density of 100%. As can be substantiated by the results presented in Fig. 9, the measured strains were also below the buckling limits.

5 Evaluation of soil pressures

The development of soil pressures within the models was evaluated in terms of the arching ratio, which is defined as the measured earth pressure normalized by the initial earth pressure at the same location before lowering the trapdoor, in vertical direction (σ_v/σ_{vo}) or in horizontal direction (σ_h/σ_{ho}). Figure 10 shows the arching ratio changes in the soil surrounding the pipe for increasing trapdoor settlements, in models built using backfills with different relative densities and subjected to an external surcharge (q) of 100 kPa. Measurements were obtained using pressure sensors located at Sections S1 and S2. For clarity, readings from only one of the two springline pressure sensors are presented in Fig. 10, as the development of pressures on either side of the pipe was essentially the same. At all circumferential positions around the pipe, active arching conditions were rapidly mobilized within the soil mass upon ground subsidence. This is confirmed by the sharp decrease in arching ratio observed even after comparatively small trapdoor settlements. Essentially, all lateral support in the pipe's springlines was lost immediately after ground subsidence (Fig. 10a). While beneficial for the crown area, stress relief is not desirable at the springlines of flexible plastic pipes, as their overall performance relies on the lateral support provided by the soil.

Unlike the results obtained for the models involving loose (D_r = 50%) and intermediate (D_r= 75%) backfills, a peak in the arching ratio was observed with the dense backfill (D_r = 100%) after an initial sharp decay at the beginning of trapdoor movement. As illustrated by the results of Model 6 shown in Fig. 3, the tested pipes showed an increase in the horizontal diameter at δ/B within the range of approximately 1% to 15%. However, the results displayed in Fig. 10a reveal that only the dense backfill was able to momentarily regain partial lateral support after subsidence, along with an increase in the diameter in the horizontal direction.

In Fig. 10a, the vertical arching ratio in the denser backfill (D_r = 100%) decreased, increased and then decreased again in response to variations in deflections in the pipe's central cross section S1. Figure 3 shows that the horizontal diameter of the model pipes firstly reduced at very small displacements, then increased and decreased once more. The initial shortening in the pipe's horizontal diameter and the trapdoor settlements induced active arching conditions in the soil mass at small displacements. Consequently, the horizontal arching ratio reduced in this phase. The subsequent increase in the pipe's horizontal diameter induced a passive arching component in the soil supporting the laterals of the pipe, and therefore, the horizontal arching ratio increased. Eventually, this passive effect was overcome by the active effect promoted by the new shortening of the horizontal diameter and the continued trapdoor settlements. The other less dense backfills (D_r = 50% and 75%) were unable to provide enough lateral support to temporarily mobilize passive arching conditions in the soil mass neighboring the pipe's springlines.

The arching ratio at the crown of the pipe exhibited an initial sharp decay at small displacements, followed by a partial recovery at larger displacements (Fig. 10b). This feature manifested at all relative densities investigated. Development of stresses at the crown of the pipe depends on the relative settlements between the zone of soil directly above the crown and in the adjacent zones. As illustrated by the radial deflection results presented in Fig. 3, the inward deflection of the pipe crown at Section S1 caused the soil on top of the pipe to settle more than the surrounding soil mass, resulting in a decreased vertical pressure in the soil at this location (active arching conditions). The subsequent recovery in the magnitude of vertical soil pressures was caused by the partial reversal of the pipe deflection at larger trapdoor settlements, also exhibited in Fig. 3.

Results of experimental models reported by Hachiya et al. [13] and Zhou et al. [44] showed an increase in the vertical pressure measured at the pipe's crown after ground subsidence, which conflicts with the findings of the present investigation. However, the problem investigated in both studies involved the subsidence of significantly wider zones below the pipe. Tests carried out by Hachiya et al.

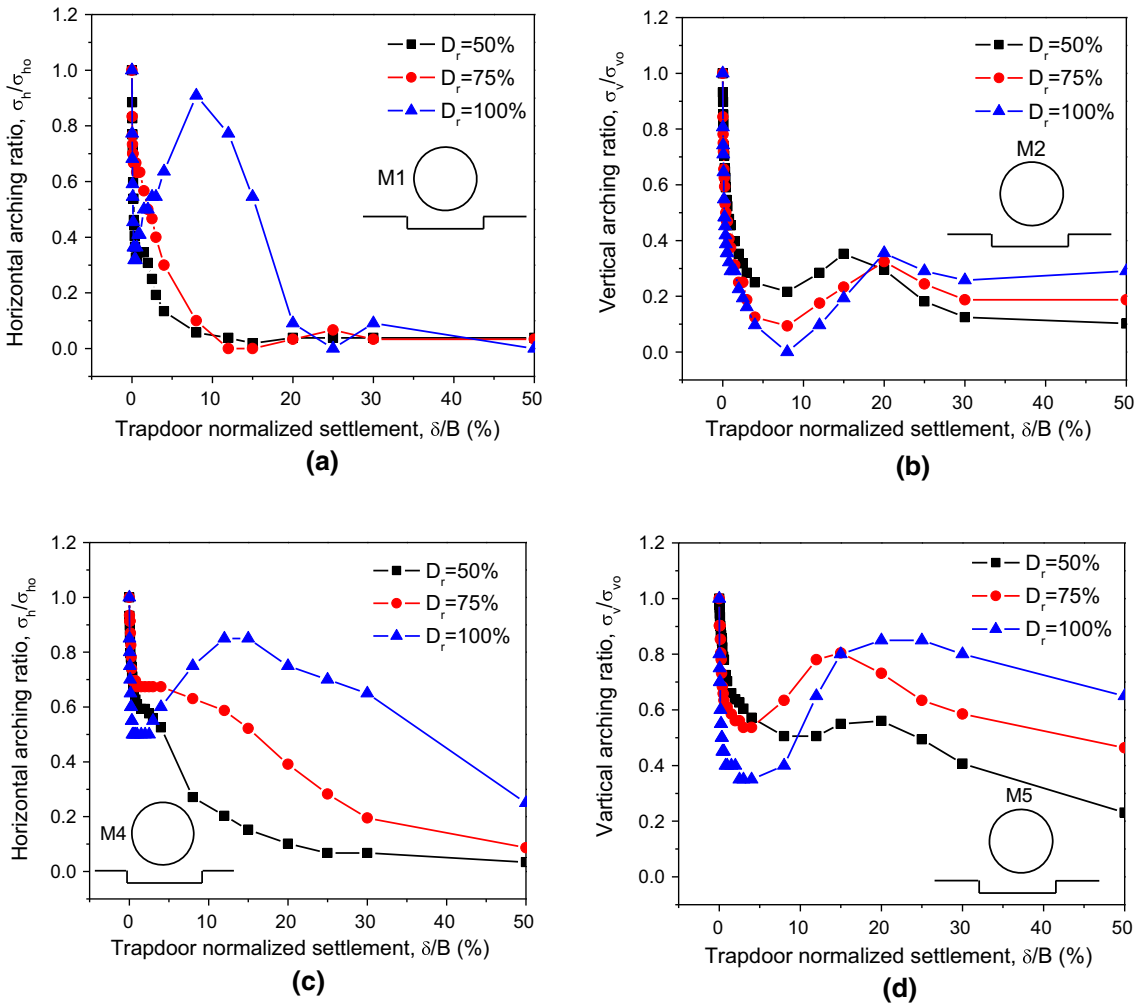

Fig. 10 Changes in the arching ratio with normalized trapdoor settlement for backfill relative densities of 50, 75 and 100%: **a** in the springline at Section S1; **b** in the crown at Section S1; **c** in the springline at Section S2; and **d** in the crown at Section S2

[13] involved models in which the subsidence zone width was equal to five pipe diameters (D), while Zhou et al. [44] considered widths of the subsidence zones ranging from 5 D to 10 D. In contrast, a width equal to 1.3 D was adopted for the models evaluated in the present study. Comparatively narrow subsidence zones beneath pipes induce a "ditch condition" in the soil [22, 33], resulting in the transfer of the load above the pipe's crown to the adjacent stable zones. However, if the width of the subsidence zone is comparatively large, active arching effects cannot develop, leading to an increase in the load acting on top of the pipe. This condition has been described as a "projection condition." The width at which ditch and projection conditions are equal has been defined as the transition width [31]. The width of the subsidence zone used in the models evaluated by Hachiya et al. [13] and Zhou et al. [44] was larger than the transition width for those cases, while the width of the subsidence zone in the models tested in the present investigation was smaller than the transition width.

As seen in Fig. 10c, d, earth pressures developed at Section S2 followed trends similar to those at Section S1. However, there were two notable differences. Firstly, the characteristic sharp decay of the arching ratio, identified in the initial segment of the curves, was comparatively smaller. Secondly, the influence of the backfill relative density at large trapdoor relative settlements was more significant. In the cases involving pipes embedded in soils of high relative density, comparatively high post-peak arching ratios were achieved.

The influence of soil confinement on the lateral support of the pipe is discussed next. Figure 11 shows the development of the arching ratio at one springline of the pipe at Section S1 for the cases of a pipe embedded in loose (D_r = 50%) and dense (D_r = 100%) soil backfills, respectively, and considering different external surcharge levels (q). The results shown in the figure indicate that soil

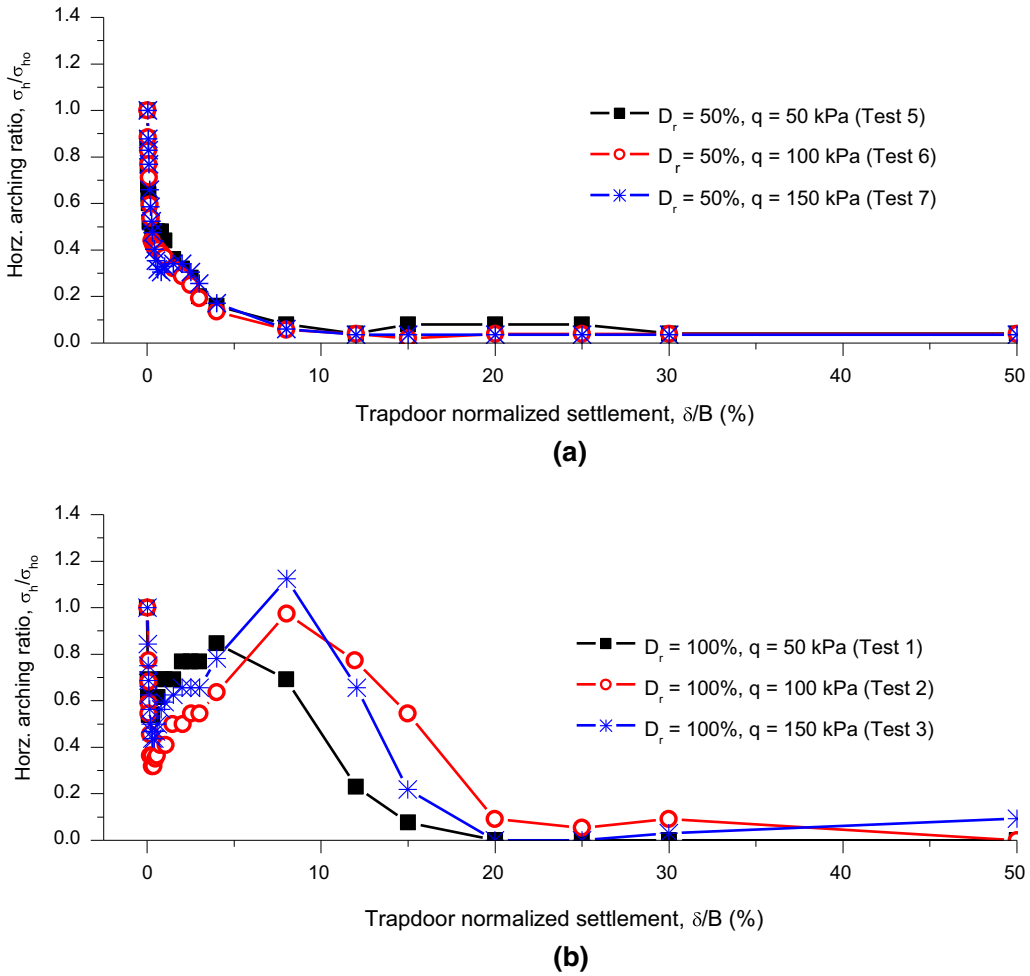

Fig. 11 Changes in arching ratio with increasing trapdoor normalized settlement at the springline of Section S1 for external surcharge values of 50, 100, and 150 kPa for: **a** a pipe embedded in loose backfill (D_r = 50%); and **b** a pipe embedded in dense backfill (D_r= 100%)

confinement did not have a significant effect in the arching ratio in the loose backfill (Fig. 11a), while that effect is more relevant in the dense backfill (Fig. 11b). In the latter case, the peak of the arching ratio follows an increasing trend with q, which occurs due to the greater lateral support against the deflection achieved by the pipe under higher confinement levels.

The vertical arching ratio at the crown of Section S1 is presented in Fig. 12a, b for different values of external surcharge (q) applied to models with loose and dense backfill soils, respectively. The peak arching ratio observed in these curves was found to be lower under high surcharge pressures. Higher confinement leads to higher arching effects at the crown of the pipe for comparatively large trapdoor settlements, consequently reducing the tendency to show high arching ratios as trapdoor settlement increases.

An estimate of the load acting on the crown of pipes undergoing subsidence can be obtained using the classic arching theory described by Terzaghi [34], modified accordingly to consider the three-dimensional nature of the problem under investigation [5]. The vertical arching ratio at the crown of a pipe having a soil cover thickness H subjected to an applied surface pressure q can be obtained as:

$$\frac{\sigma_v}{\sigma_{vo}} = \frac{\gamma}{2\sigma_{vo}K\tan\phi w}\left[1 - e^{-2K\tan\phi wH}\right] + \frac{q}{\sigma_{vo}} \cdot \left[e^{-2K\tan\phi wH}\right] \quad (4)$$

where γ is the soil unit weight; K is the lateral earth pressure coefficient; w is a geometry coefficient; and ϕ is the soil internal friction angle, obtained from triaxial test results with the tested sand, as reported in Costa and Zornberg [9]. The other parameters have been defined previously.

In the theory, shear stresses within the soil are assumed to develop along vertical planes that initiate at the trapdoor edges and reach the ground surface. The geometry coefficient (w) equals ($1/B + 1/L$), where B is the trapdoor width and L is the trapdoor length. The arching ratio calculated

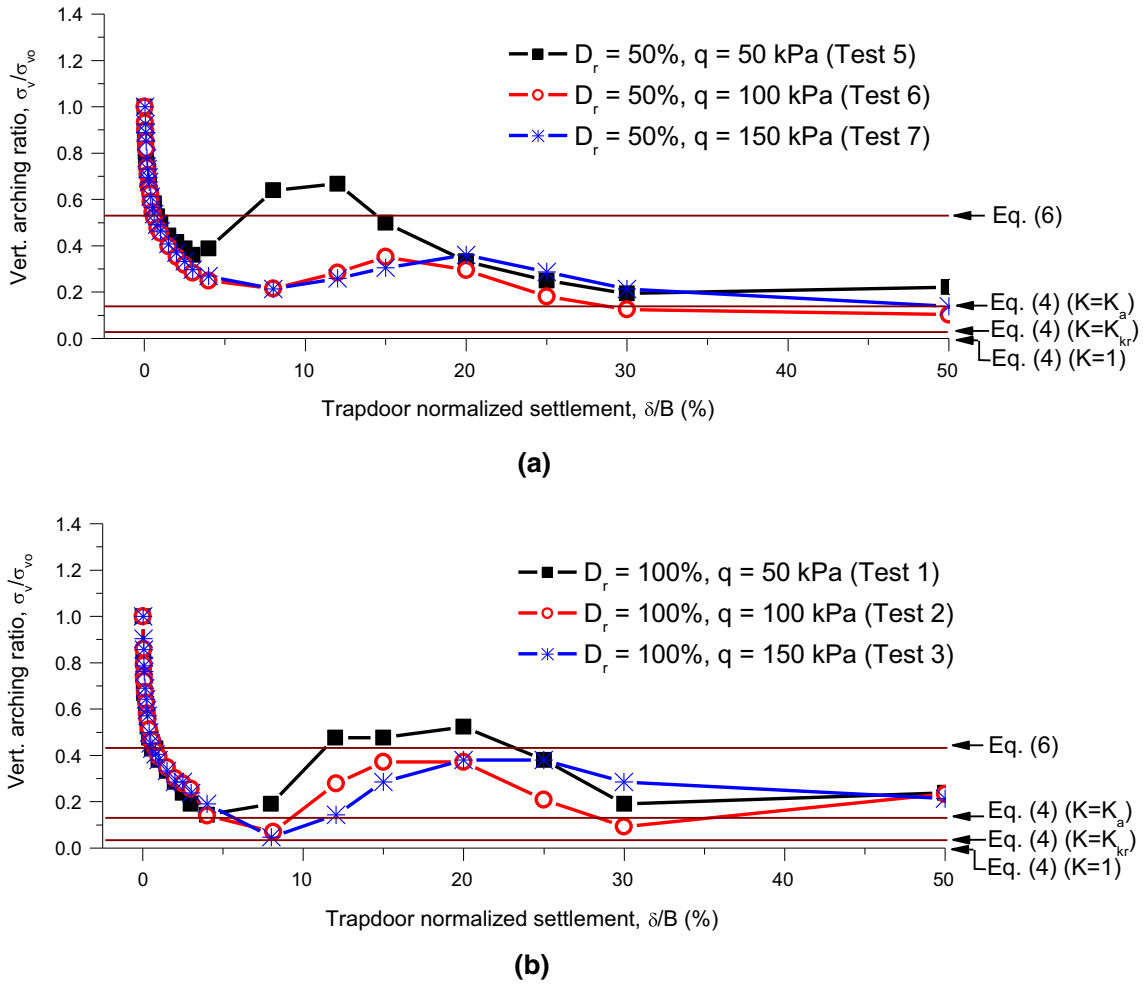

Fig. 12 Changes in vertical arching ratio with increasing normalized trapdoor settlements at the crown of Section *S1* for external surcharges of 50, 100, and 150 kPa for: **a** a pipe embedded in loose backfill (D_r= 50%); and **b** a pipe embedded in dense backfill (D_r = 100%)

using Eq. (4) represents the ultimate state of the soil arching process, corresponding to large trapdoor normalized settlements, where vertical shear planes propagate in the soil mass [16, 17].

Several criteria have been proposed to select the lateral earth pressure coefficient (K) used in Eq. (4). Marston and Anderson [22] and Spangler [33] recommended using Rankine's active earth pressure coefficient (K_a). Strictly, the hypothesis of $K = K_a$ implies an absence of frictional resistance along the hypothetical vertical planes, which is unrealistic. In actuality, friction causes rotation of the principal stresses along the slip surfaces. Using a demonstration involving Mohr's circles, Krynine [20] proposes calculating K on the surface of a rough wall as follows:

$$K = K_{kr} = \frac{1 - \sin^2 \emptyset}{1 + \sin^2 \emptyset} \tag{5}$$

Krynine's [20] approach yields values that are larger than those corresponding to Rankine's theory. Some experimental results indicated that the earth pressure coefficient reaches values ranging from 1 to 1.6 [19, 35]. Specifically, from laboratory tests, Evans [10] found that the horizontal earth pressures in the soil above a trapdoor remain practically constant with increasing trapdoor settlements, rather than decreasing along with the decreasing vertical pressures. This caused K to reach a maximum value of 1.2 for a normalized vertical settlement (δ/B) of 1%.

Table 2 Summary of predicted arching ratios obtained with Eq. (4)

Model test	D_r (%)	q (kPa)	Arching ratio, σ_v/σ_{vo}		
			$K = 1$	$K = K_{kr}$	$K = K_a$
1	100	50	0.015	0.05	0.15
2	100	100	0.008	0.03	0.13
3	100	150	0.006	0.02	0.12
5	50	50	0.014	0.04	0.15
6	50	100	0.008	0.03	0.12
7	50	150	0.005	0.02	0.11

The impact of the lateral earth pressure coefficient K on the soil-arching ratio was investigated by adopting K values equal to 1, K_a and K_{kr} in Eq. (4). Predictions of the arching ratio obtained from Eq. (4) are listed in Table 2. Predictions are compared with the experimental results by horizontal lines in Fig. 12a, b. For clarity, only the average value for each backfill density is represented in the figures, as very similar results were obtained for the range of surcharges (q) investigated. Predictions with $K = 1$ yielded negligible arching ratios resulting in a horizontal line that overlaps with the horizontal axis of the graph. Predicted arching ratios are compared with the maximum values recorded at the crown of each model pipe. This approach is consistent with the fact that this analytical solution involves assuming large displacements of the underground structure, above 10% B [14]. Arching ratios calculated using Eq. (4) resulted in underestimated predictions of the experimental maximum arching ratio. Predictions were not significantly affected by the assumed K value. However, the best match with the experimental values was obtained assuming $K = K_a$ for both loose and dense backfill conditions.

An additional prediction of the arching ratio at the crown of the settling pipe was carried out using Eq. (6), recommended by AASHTO [1]. The aim of this second analysis was to assess the suitability of currently used methods for the design of buried pipelines applied considering the specific case of ground loss of support:

$$\frac{\sigma_v}{\sigma_{vo}} = 0.76 - \frac{0.71(S_H - 1.17)}{(S_H - 2.92)} \quad (6)$$

where S_H is the hoop stiffness factor, given by Eq. (7):

$$S_H = \frac{\emptyset_s M_s R}{E_p A} \quad (7)$$

where ϕ_s is the resistance factor for soil stiffness (set to 0.9 [1]); M_s is the constrained soil modulus; R is the radius from the center of the pipe to the centroid of the pipe profile; E_p is the Young's modulus of pipe material; and A is the gross area of pipe wall per unit length of pipe.

Table 3 Parameters used in AASHTO's [1] method and calculated arching ratios

Model test	D_r (%)	q (kPa)	M_s (MPa)	Arching ratio, σ_v/σ_{vo}
1	100	50	26.1	0.43
2	100	100	33.0	0.41
3	100	150	39.1	0.40
5	50	50	3.7	0.53
6	50	100	4.2	0.53
7	50	150	4.6	0.52

Table 3 lists the arching ratios obtained from Eq. (6). The constrained soil modulus (M_s) used in Eq. (7), selected from the range of values recommended in the method outlined by AASHTO [1], is also listed in Table 2. Predictions from Eq. (6) are shown with horizontal lines in Fig. 12a, b. Similarly to the previous method, the average value for each backfill density is represented by a single line if Fig. 12a, b, as very similar predictions were achieved for the range of surcharges (q) examined.

Results obtained using Eq. (6) were found to be more conservative than those obtained using Eq. (4), as shown in Fig. 12a, b. Values predicted with Eq. (6) exceeded the experimental maximum arching ratios obtained with the higher surcharge levels tested and were slightly below the ratios obtained with the lower surcharge level tested. Generally, predictions made with Eq. (4) more closely approached the range of recorded experimental minimum arching ratios, while estimates given by Eq. (6) were closer to the range of measured experimental maximum arching ratios.

Variations in earth pressures below the pipe are discussed next. In all tested models, vertical earth pressures below the pipe reduced in positions I1 and I2 and increased in positions I3 and I4, as a consequence of the settlements promoted by the trapdoor. Figure 13 presents the minimum arching ratio recorded at positions I1 and I2 and the maximum arching ratio recorded at positions I3 and I4 in each model. It is noted that the vertical earth pressures increased considerably in the bedding layer below the pipe segment beyond a distance of about 1 D outside the subsidence zone, exceeding, in some cases, the initial vertical pressure by nearly 50%.

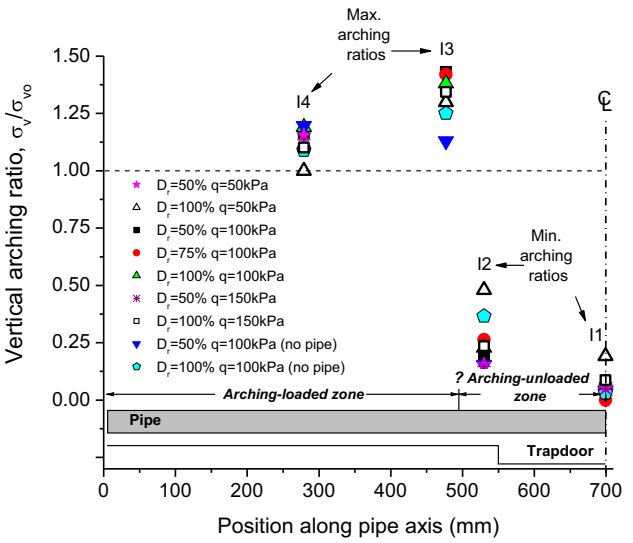

Fig. 13 Summary of vertical arching ratio data obtained below the pipe at different locations along the pipe axis

Using results obtained from the models without pipes as reference, the earth pressure measurements at position I3 reveal that the presence of the pipe promoted an additional load transfer from the unstable collapsing region over the trapdoor to the stable region of the soil mass. Due to the absence of bedding support, the load at the top of the segment of pipe spanning the subsidence zone was transferred by the pipe to the segment in the stable soil mass. As illustrated by the results shown in Fig. 5, position I3 was located below a region of the pipe invert that experienced large deflections, so that accommodations of the invert after subsidence may have contributed to the increase in vertical earth pressures below the pipe.

6 Discussion on the PVC pipe performance

An analysis of the deflection response of the model pipes shows that an adequate soil compaction increases the chances that the PVC pipe will remain operational after a potential localized ground subsidence event. Possible damage to the pipe can be reduced with a well-compacted backfill. Since more support is offered by a stiffer soil around the pipe, less of the soil self-weight and external loads needs to be resisted by the pipe. Also, an analysis of the effect of the levels of soil confinement applied to the models suggests that deeper PVC pipe installations are likely to suffer more from the effects of a localized ground loss of support than shallower installations.

Although significant bending developed in the segment of the model PVC pipes bridging the subsidence zone, recommended performance limits by AASHTO [1] for deflections and wall strains of flexible pipes were satisfied in this study. However, while the analysis did not indicate that the loss of support would compromise the performance and capabilities of the pipe, it showed that part of the pipe's ability to remain operational was exhausted by bridging the void, thus reducing its capacity to accommodate other conventional design requirement demands. It is also notable that a jointed PVC pipe experiencing equivalent subsidence conditions could reach serviceability limits due to misalignment and thereby compromise joint tightness, which warrants further investigation.

As discussed by Costa and Zornberg [9], an active trapdoor develops an arching-unloaded region in the soil mass, where stresses decrease, and an arching-loaded region beyond the limits of the trapdoor, where stresses are transferred to. The arching-unloaded region includes part of the soil mass outside the trapdoor footprint, where a more moderate decrease in vertical stresses occurs. The changes in vertical earth pressures recorded at the floor of the pipe models due to soil arching indicate that the boundary between both regions is located somewhere between positions I2 and I3 (Fig. 13), which corresponds to a horizontal distance between 0.3 D and 1 D from the edge of the trapdoor. Consequently, the length of the pipe segment undergoing loss of support is about 1.15 to 1.5 times larger than that of the subsidence zone (trapdoor). However, this is important to emphasize that this length should depend on the thickness of the bedding layer below the pipe.

The interface zone between the arching-unloaded and arching-loaded regions separates the pipe segments fixed to the stable soil mass from the central, unsupported segment bridging the arching-unloaded region. High shear forces that can lead to wall deformations are expected in the sections of the pipe intersecting the interface zone. Additionally, the load from the unsupported pipe segment that is transferred to the fixed pipe segment is more concentrated closer to the interface zone, as suggested by the vertical pressure measurements in Fig. 13. In effect, comparatively large radial deflections of the pipe invert, at a distance of about 1 D from the trapdoor edge, were recorded with model pipes embedded in loose backfills, as illustrated in Fig. 4.

The changes in vertical earth pressures in the soil beneath the pipe (Fig. 13) also reveal that the soil–pipe interaction involves slippage conditions at the pipe segment bridging the arching-unloaded region. This is an important detail for numerical and analytical modeling of buried pipe performance under comparable subsidence conditions. To adequately model soil–pipe behavior, shear stresses developing at the soil–pipe interface during slippage need to be taken into consideration. Furthermore, due to the separation that occurs between the pipe and soil, the displacement of the pipe cannot be assumed to equal the settlement of the underlying soil, as is the case for beam–spring models.

7 Summary and conclusions

A series of laboratory model tests was carried out to assess the response of polyvinyl chloride (PVC) pipes to subsidence of a localized area of the supporting soil. Ground subsidence below the pipe was simulated by a rectangular trapdoor with a length of 4 D and a width of 1.3 D (where D is the pipe diameter). A technique including the use of a custom-made strain gage-based displacement transducer was developed for recording continuous radial deflection profiles along the axis of the model pipes. Pressure variations in the soil mass and pipe wall strains were also monitored and analyzed. The effects of backfill density and soil confinement level on pipe performance were investigated. Based on the results of the present study, the following conclusions can be drawn:

(1) The displacement transducer fabricated as part of this study was found to provide consistent radial deflection profiles of the model pipes tested. The deflection profiles showed that the pipe deformed under lateral and bottom losses of support.
(2) The pipe crown experienced the largest deflections due to ground subsidence. Deflections were higher at the pipe middle span and gradually attenuated toward the pipe edges. Most variations in pipe deflections occurred within a settlement of about 15% of the width of the subsidence zone (B).
(3) Deflections were found to be very sensitive to the density of the backfill soil. While pipe deflections remained low with dense and medium-dense backfills, they grew significantly with loose backfills. In the latter case, significant bending developed in the pipe segment traversing the subsidence zone as trapdoor settlement increased. Sagging of the crown, upheaval of the invert and extension of the horizontal diameter were identified in the pipe. Deflections in pipes embedded in loose backfill extended along the pipe length to a distance of about 4 D beyond the boundary of the subsidence zone.
(4) Although increasing soil confinement contributed to substantial growth in deflections of pipes embedded in loose backfill, the effect was small in dense and medium-dense backfills.
(5) Data of strains recorded in the external pipe wall during subsidence revealed that pipes embedded in loose backfill achieved comparatively higher strain levels in both longitudinal and circumferential directions.
(6) Ground subsidence induced mobilization of active arching conditions in the soil surrounding the pipe, with load transferred from the region above the subsidence zone to farther regions of the backfill. Vertical earth pressures increased considerably in the bedding layer below the pipe segment beyond a distance of about 1 D outside the subsidence zone, exceeding, in some cases, the initial vertical pressure by nearly 50%. The length of the pipe segment that suffers loss of support was estimated to be within a range between 1.15 and 1.5 times the length of the subsidence zone (trapdoor).
(7) Predictions made with the calculation method proposed by AASHTO [1] for conventional design of buried pipelines provided reasonable agreement with the maximum vertical earth pressure recorded at the crown of the PVC pipes undergoing a localized subsidence. On the other hand, estimates obtained from the three-dimensional soil arching theory derived from the formulation by Terzaghi [34] more closely corresponded to the range of minimum vertical earth pressures collected from the physical models.

The results of the present investigation indicate that the quality of the compaction of the soil envelope plays an important role on the performance of a PVC pipe undergoing loss of localized support. Potential damages in pipes undergoing loss of localized support can be reduced with a well-compacted soil envelope.

In the case considered herein, recommended performance limits for deflections and wall strains of flexible pipes were satisfied. While the analysis did not indicate that the loss of support would compromise the performance and capabilities of the pipe, it showed that part of the pipe's ability to remain operational was exhausted by bridging the void, thus reducing its capacity to accommodate other conventional design requirement demands. However, additional investigations involving other conditions, including the presence of joints, are necessary to further elucidate the soil–pipe interactions involved.

Acknowledgements The authors express their gratitude to Prof. Benedito S. Bueno (*in memoriam*) for his valuable assistance in the development of this work. The authors are also thankful to the Geotechnical Engineering Department of the University of São Paulo at São Carlos, Brazil, and the Civil Engineering Department of the University of Colorado at Boulder, USA, where the first part of this investigation was conducted. Financial support to this research was provided by the Research Foundation of the State of São Paulo, Brazil (FAPESP) (Grant No. 00/09397-0).

References

1. American Association of State Highway and Transportation Officials (AASHTO) (2012) AASHTO LRFD bridge design specifications, 2nd edn, Sec. 12, Washington, DC
2. ASTM (2011) Standard test method for determination of external loading characteristics of plastic pipe by parallel-plate loading—D2412-11, annual book of ASTM standards. ASTM International, West Conshohocken
3. Balkaya M, Moore ID, Saglamer A (2012) Study of non-uniform bedding due to voids under jointed PVC water distribution pipes. Geotext Geomembr 34:39–50. https://doi.org/10.1016/j.geotexmem.2012.01.003
4. Benmansour A, Abdallah A, Masrouri F, Auvinet G (1997) Analyse fiabiliste du comportement axial des conduits d'assainissement. Can Geotech J 34:329–343
5. Brachman RWI, Moore ID, Rowe RK (2000) The design of a laboratory facility for evaluating the structural response of small-diameter buried pipes. Can Geotech J 37:281–295
6. Bransby MF, Nahas ELA, Turner E, Davies MCR (2007) The interaction of reverse faults with flexible continuous pipelines. Int J Phys Model Geotech 7(3):25–40
7. Cohen BR (2012) Fixing America's crumbling underground water infrastructure. Competitive Enterprise Institute. https://cei.org/issue-analysis/fixing-americas-crumbling-underground-water-infrastructure. Accessed 14 Jan 2019
8. Costa YD, Zornberg JG, Bueno BS, Costa CL (2009) Failure mechanisms in sand over a deep active trapdoor. J Geotech

Geoenviron Eng 135(11):1741–1753. https://doi.org/10.1061/(ASCE)GT.1943-5606.0000134
9. Costa YDJ, Zornberg JG (2020) Active and passive arching stresses outside a deep trapdoor. Acta Geotech. https://doi.org/10.1007/s11440-020-00969-x
10. Evans CH (1983) An examination of arching in granular soils. M.S. thesis, Massachusetts Institute of Technology, Cambridge
11. Folkman S (2018) Water main break rates in the USA and Canada: a comprehensive study. Mechanical and Aerospace Engineering Faculty Publications, Paper 174. https://digitalcommons.usu.edu/mae_facpub/174. Accessed 24 Jan 2019
12. Guo S, Shao Y, Zhang T, Zhu D, Zhang Y (2013) Physical modeling on sand erosion around defective sewer pipes under the influence of groundwater. J Hydraul Eng 139(12):1247–1257. https://doi.org/10.1061/(ASCE)HY.1943-7900.0000785
13. Hachiya M, Inoue Y, Tohda J, Takatsuka Y, Takagi R (2002) Response of buried pipelines subjected to differential ground settlement. In: Proceedings of the physical modeling in geotechnics (ICPMG'02), Swets & Zeitling Lisse, pp 911–916
14. Han J, Wang F, Al-Naddaf M, Xu C (2017) Progressive development of two-dimensional soil arching with displacement. Int J Geomech 17(12):04017112. https://doi.org/10.1061/(ASCE)GM.1943-5622.0001025
15. Handy RL, Spangler MG (2007) Geotechnical engineering: soil and foundation principles and practice, 5th edn. McGraw-Hill, New York
16. Iglesia GR, Einstein HH, Whitman RV (1999) Determination of vertical loading on underground structures based on an arching evolution concept. In: Fernandez G, Bauer RA (eds) Geo-engineering for underground facilities. ASCE, Reston, pp 495–506
17. Iglesia GR, Einstein HH, Whitman RV (2014) Investigation of soil arching with centrifuge tests. J Geotech Geoenviron Eng 137(11):1075–1080. https://doi.org/10.1061/(ASCE)GT.1943-5606.0000998
18. Indiketiya S, Jegatheesan P, Rajeev P, Kuwano K (2019) The influence of pipe embedment material on sinkhole formation due to erosion around defective sewers. Transp Geotech 19:110–125. https://doi.org/10.1016/j.trgeo.2019.03.001
19. Krizek RJ, Parmelee RA, Kay J, Elnagger H (1971) Structural analysis and design of pipe culverts. National Cooperative Highway Research Program Report, 116, HRB
20. Krynine DP (1945) Stability and stiffness of cellular cofferdams. Trans ASCE 110:1175–1178 **(discussion)**
21. Marshall AM, Klar A, Mair RJ (2010) Tunneling beneath buried pipes: view of soil strain and its effect on pipeline behavior. J Geotech Geoenviron Eng 136(12):1664–1672. https://doi.org/10.1061/_ASCE_GT.1943-5606.0000390
22. Marston A, Anderson AO (1913) The theory of loads on pipes in ditches and tests of cement and clay drain tile and sewer pipe. Bul. 31, Iowa Eng. Expt. Station
23. Moser AP, Folkman S (2008) Buried pipe design, 3rd edn. McGraw-Hill, New York City
24. O'Rourke M, Gadicherla V, Abdoun T (2005) Centrifuge modeling of PGD response of buried pipe. Earthq Eng Eng Vibr 4(1):69–73
25. Peng SS, Luo Y (1988) Determination of stress field in buried thin pipelines resulting from ground subsidence due to longwall mining. J Min Sci Technol 6(2):205–216
26. Peter JM, Chapman D, Moore I, Hoult N (2018) Impact of soil erosion voids on reinforced concrete pipe responses to surface loads. Tunn Undergr Space Technol 82:111–124. https://doi.org/10.1016/j.tust.2018.08.003
27. Rajani B, Zhan C, Kuraoka S (1996) Pipe-soil interaction analysis of jointed water mains. Can Geotech J 33:393–404
28. Saiyar M, Ni P, Take WA, Moore ID (2016) Response of pipelines of differing flexural stiffness to normal faulting. Géotechnique 66(4):275–286. https://doi.org/10.1680/jgeot.14.P.175
29. Saiyar M, Take W, Moore I (2011) Validation of boundary PIV measurements of soil–pipe interaction. Int J Phys Modell Geotech 11(1):23–32. https://doi.org/10.1680/ijpmg.2011.11.1.23
30. Santichaianant K (2002) Centrifuge modeling and analysis of active trapdoor in sand. Ph.D. Thesis, University of Colorado at Boulder
31. Schlick WJ (1932) Loads on pipe in wide ditches. Bulletin 108, Iowa State, Engineering Experiment Station
32. Shen SL, Xu YS (2011) Numerical evaluation of land subsidence induced by groundwater pumping in Shanghai. Can Geotech J 48(9):1378–1392. https://doi.org/10.1139/t11-049
33. Spangler MG (1950) Theory of loads on negative projecting conduits. Proc HRB 30:153–161
34. Terzaghi K (1943) Theoretical soil mechanics. Wiley, New York
35. Terzaghi K (1936) Stress distribution in dry and saturated sand above a yielding trap-door. In: Proceedings of the 1st intl conference on soil mechanics and foundation engineering, Cambridge, Mass, pp 35–39
36. Tohda J, Hachiya M (2005) Response and design of buried pipelines subjected to differential ground settlement. In: Proceedings of the 16th intl conference on soil mechanics and geotechnical engineering. Millpress Science Publishers/IOS Press, pp 1659–1662
37. Vorster TEB, Klar A, Soga K, Mair RJ (2005) Estimating the effects of tunneling on existing pipelines. J Geotech Geoenviron Eng 131(11):1399–1410
38. Wang F, Du YJ, Yang XM (2015) Physical modeling on ground responses to tunneling in sand considering the existence of HDPE pipes. Geotech Test J 38(1):85–97. https://doi.org/10.1520/GTJ20140031
39. Wang B, Li X, Zhou J (2011) Strain analysis of buried steel pipelines across strike-slip faults. J Cent South Univ Technol 18(5):1654–1661
40. Wang X, Shuai J (2009) Stress and strain analysis of buried pipeline subject to mine subsidence. In: Najafi M, Ma B (eds) Advances and experiences with pipelines and trenchless technology for water, sewer, gas, and oil applications. ASCE, Reston, pp 1219–1228
41. Watkins RK, Anderson LR (1999) Structural mechanics of buried pipes. CRC Press, Boca Raton
42. White DJ, Take WA, Bolton MD (2003) Soil deformation measurement using particle image velocimetry (PIV) and photogrammetry. Géotechnique 53(7):619–631. https://doi.org/10.1680/geot.2003.53.7.619
43. Wols BA, van Thienen P (2014) Modelling the effect of climate change induced soil settling on drinking water distribution pipes. Comput Geotech 55:240–247
44. Zhou M, Wang F, Du Y-J, Liu MD (2019) Laboratory evaluation of buried high-density polyethylene pipes subjected to localized ground subsidence. Acta Geotech 14(4):1081–1099. https://doi.org/10.1007/s11440-018-0698-6

Publisher's Note Springer Nature remains neutral with regard to jurisdictional claims in published maps and institutional affiliations.